Agricultural and Forest Meteorology 268 (2019) 55–62

Contents lists available at ScienceDirect

Agricultural and Forest Meteorology

journal homepage: www.elsevier.com/locate/agrformet

Growth stage-dependant variability in water vapor and CO_2 exchanges over a humid alpine shrubland on the northeastern Qinghai-Tibetan Plateau

Hongqin Li[a,b,1], Jingbin Zhu[b,d,1], Fawei Zhang[a,b,c,*], Huidan He[b,d], Yongsheng Yang[b], Yingnian Li[b,c,*], Guangmin Cao[b], Huakun Zhou[b,c]

[a] College of Life Sciences, Luoyang Normal University, Luoyang, Henan, 471934, China
[b] Key Laboratory ofAdaptation and Evolution of Plateau Biota, Northwest Institute of Plateau Biology, Chinese Academy of Sciences, Xining, Qinghai, 810001, China
[c] Qinghai Provincial Key Laboratory of Restoration Ecology in Cold Region, Northwest Institute of Plateau Biology, Chinese Academy of Sciences, Xining, Qinghai, 810001, China
[d] University of Chinese Academy of Sciences, Beijing, 100049, China

ARTICLE INFO

Keywords:
Net ecosystem CO_2 exchange
Evapotranspiration
Biotic controls
Structural equation models
Eddy covariance techniques
Humid alpine shrubland

ABSTRACT

Large uncertainties exist in carbon-water-climate feedbacks in cold regions, partly due to an insufficient understanding of the simultaneous effects of climatic and biotic controls on water and carbon dynamics. The 10-year growing season flux data were analyzed to evaluate the relative contributions of climatic and biotic effects on the variability of water vapor (*ET*) and net ecosystem CO_2 (*NEE*) exchanges over a humid alpine deciduous shrubland on the northeastern Qinghai-Tibetan Plateau. The results showed that the alpine shrubland ecosystem acted as a water source and a carbon sink during the growing season, and its potential *ET* and *NEE* ranged from 161.4 mm and –41.0 g C·m^{-2} to 408.0 mm and –278.4 g C·m^{-2} at a 95% confidence interval, respectively. The average 8-day *ET* and *NEE* during the early growing season (June to July) were both significantly ($P < 0.05$) more than those of the late growing season (August to September). And the slopes of *ET* and *NEE* against the Julian day during the two growth stages also changed significantly ($P < 0.01$). Such asymmetric manners of *ET* and *NEE* during the two growth stages were probably related to the seasonal variations of net radiation (*Rn*) and vegetation growth (satellite-derived enhanced vegetation index: *EVI*), respectively. The structural equation models showed that the seasonal variations of 8-day *ET* were jointly determined by *Rn* and vapor pressure deficit (*VPD*), as partly indicated by a modest decoupling coefficient (0.54 ± 0.03). The seasonal variability in 8-day *NEE* was controlled by the combinations of *EVI* and growing season degree days (*GDD*). The standardized coefficient of the direct effect of *EVI* on *ET* was 0.16, much less than the corresponding value (0.51) on *NEE*, suggesting that a weak coupling between *ET* and *NEE* arose likely because water vapor loss were about half controlled by surface evaporation, whereas CO_2 flux were largely regulated by vascular plant activity. Our results highlighted the asymmetric sensitivities of *ET* and *NEE* during the early and the late growing season, and the weak coupling of water loss and carbon fixation during the whole growing season. These findings would provide a new sight to understand the growth stage-dependent responses of water budget and carbon sequestration to grazing management and climate change in humid alpine shrublands.

1. Introduction

Alpine grasslands act as the headwaters of the lowlands and, as large stores of soil organic carbon, are highly sensitive and vulnerable to ongoing climate change (Körner, 2003; Knowles et al., 2012; Li et al., 2017). And their responses have the potential to impact the local climate system through several feedbacks, such as the short-term energy partitioning strategy and the long-term carbon sequestration capacity (McGuire et al., 2002; Richardson et al., 2013; Ueyama et al., 2013). The ongoing climate warming and altered precipitation regimes have substantially influenced the highland ecohydrological processes and resultant water supply capacity (Vourlitis and Oechel, 1999; Chapin et al., 2005; Blok et al., 2011; Iwata et al., 2012). The balance between the aroused large soil CO_2 release and synchronous enhanced vegetation CO_2 uptake under warm conditions determines the direction and magnitude of ecosystem carbon function (Shen et al., 2015; Li et al.,

* Corresponding authors at: 6#, Jiqing Streets, Yibin Districts, 471934 Luoyang, Henan, China.
E-mail addresses: mywing963@126.com (F. Zhang), ynli@nwipb.cas.cn (Y. Li).
[1] These authors contribute equally

https://doi.org/10.1016/j.agrformet.2019.01.013
Received 26 July 2018; Received in revised form 5 December 2018; Accepted 8 January 2019
Available online 11 January 2019
0168-1923/ © 2019 Elsevier B.V. All rights reserved.

2016; Rogers et al., 2017). Accurate understanding of the mechanism in water vapor and CO_2 dynamics and their environmental controls in alpine regions can allow useful estimates of water and carbon budgets on reasonable temporal and spatial scales (McFadden et al., 2003) and thus, predictions of the future role in regional water management and climate change (Le Quéré et al., 2009; Teuling et al., 2010; Ueyama et al., 2013). In recent decades, the importance of water conservation and carbon sequestration has been increasingly acknowledged while the underlying processes remains unclear, probably due to the harsh environment and associated lack of multi-year robust observations in high altitude areas (McFadden et al., 2003; Gu et al., 2008; Ueyama et al., 2014).

The surface-atmosphere exchanges of water vapor (*ET*) and CO_2 (*NEE*) during the growing season accounts for the most proportions of water and carbon budgets in alpine ecosystems (McFadden et al., 2003; Ueyama et al., 2013; Li et al., 2016). The seasonal *ET* is more derived from the surface (mosses, soil (McFadden et al., 2003; Blok et al., 2011), and canopy interception (Wang et al., 2012)) evaporation or vegetation biological transpiration (Kelliher et al., 1995; Hu et al., 2009). So *ET* variability is mainly determined by radiation energy availability (Iwata et al., 2012; Knowles et al., 2012; Zhang et al., 2018) or surface moisture conditions (atmospheric humidity deficit and soil water content (Teuling et al., 2010; Ma et al., 2015)). Meanwhile, seasonal *NEE* is generally controlled by thermal conditions (Kato et al., 2006; Ueyama et al., 2013; Li et al., 2016), moisture status (Teuling et al., 2010; Chen et al., 2016), vascular plant amounts and activity (McGuire et al., 2002; McFadden et al., 2003), and canopy nutrient concentrations (Chapin et al., 2011; Rogers et al., 2017). These simultaneous changes in climatic controls and biotic variables regulate the variability in *ET* and *NEE* but the relative contribution varies by vegetation types, climate conditions and growth stages and is not well quantified (McGuire et al., 2002; Shao et al., 2015; Li et al., 2017). And then a strong linkage (Hu et al., 2009; Richardson et al., 2013) and poor coupling (Vourlitis and Oechel, 1999; McFadden et al., 2003) between *ET* and *NEE* has both been observed in alpine grasslands. However, to our knowledge, few studies have distinguished the relative importance of climatic drivers and biotic controls on growing season *ET* and *NEE* variability (Shao et al., 2015). Addressing this issue will be helpful in reducing uncertainty in quantitative contributions to regional water resource and climate change.

To address the issue, we analyzed the 10-year continuous time series of growing season *ET* and *NEE* and environmental controls over a humid alpine deciduous shrubland on the northeastern Qinghai-Tibetan Plateau (QTP). The alpine shrubland is one of the most common vegetation types on the highlands and generally occupies relatively cold-humid regions, such as the shady or semi-shady slopes of mountains and the alluvium and diluvium on plains beneath snowpack mountains. The alpine shrubland thus plays much sensitive function in water availability and carbon sequestration in cold areas due to the relatively higher location (Zheng et al., 2000; Körner, 2003; Li et al., 2016). We focused firstly on quantifying the seasonal patterns in *ET* and *NEE,* secondly on distinguishing the relative contributions of climatic drivers and biotic controls. Based on the findings that *ET* is determined by the radiation energy availability (Knowles et al., 2012; Zhang et al., 2018) while *NEE* is mainly controlled by thermal conditions and associated vegetation status (Ueyama et al., 2013; Li et al., 2016), we hypothesized that *ET* and *NEE* might be weakly coupled in the humid alpine shrubland.

2. Material and methods

2.1. Site descriptions

The study was conducted on a humid alpine shrubland, about 10 km north of the Haibei National Field Research Station for Alpine grassland (Haibei Station, 37°37′ N, 101°19′ E, 3200 m a.s.l.). Haibei Station is a member of China Flux Observation and Research Network. The study site landscape is characterized by deciduous shrub (*Potentilla fruticosa*) with an understory of vascular plants, including *Kobresia humilis*, *Polygonum viviparum*, *Stipa aliena*, *Poa orinosa*, *Helictotrichon tibeticum*, *Elymus nutans*, *Aster flaccidus*, *Polygonumviviparum*, and *Leontopodium nanum*. The surface texture is more heterogeneous at the shrubland and extended vegetated patches interchanges with bare soil overlying moss. The mean shrub coverage and canopy height are ca. 60% and ca. 50 cm, respectively. Mean annual temperature is –1.3 °C and precipitation is 461.0 mm, with more than 75% falling as rain during the growing season from June to September. The soil is predominately sandy loam, with a topsoil composition of 59.8% loam, 34.3% sand and 5.9% clay, and generally classified as Mollic Gryic Cambisols. The study site is underlain by permafrost which extends to a depth of ca. 6.0 m and moderately (3.75 sheep·ha^{-1}) grazed by yaks and Tibetan sheep from early October to mid-May (Li et al., 2014).

The vegetative growth and reproductive growth of most plant species in the alpine shrubland is mainly concentrated in June to July and August to September, respectively (Li et al., 2016). Then the growing season was divided into two stages: the early growing season (June to July) and the late growing season (August to September). The specific flag date splitting the two growth stages was a little different for *ET* and *NEE*, according to the results of a piecewise linear regression (Fig. 2).

2.2. Flux instrumentation and environmental controls

In September 2002, the flux tower has been installed in the center of a flat (slope < 1%) site, with a uniform vegetation cover (shrub coverage 60%) over a fetch of 12 km^2, and open distance of ca. 5 km minimum between the mountain foot and the opposite highway. Data from 2003 to 2012 were used in this study. *ET* and *NEE* were measured by the eddy covariance techniques, which consisted of a three-dimensional ultrasonic anemometer (CSAT3, Campbell, USA) and an open-path infrared CO_2/H_2O gas analyzer (LI-7500, LI-Cor, USA) at a height of 2.2 m above the ground. Therefore, the changes of storage item below the measuring height were negligible because of the low height of the shrub canopy (McFadden et al., 2003). Continuous high-frequency (10 Hz) raw data were recorded and half-hourly flux data were calculated with appropriate corrections (Li et al., 2016). The routine meteorological variables, such as daily air temperature (T_a, including maximum temperature: T_{max}, minimum temperature: T_{min}), relative humidity (*RH*), wind velocity (*Ws*), incident solar radiation (*DR*), net radiation (*Rn*), precipitation (*Rain*), 10 cm volumetric soil water content (*SWC*) and 5 cm soil heat flux (*G*) were also synchronously monitored. Further details of the measurement system have been provided by Li et al. (2014; 2016). The averaged daily energy closure ratio (defined as the ratio between the turbulent heat fluxes against the difference of net radiant fluxes with soil heat fluxes) was 0.76 (from 0.66 in 2012 to 0.83 in 2017, Fig. S1), indicated that flux measurements were reasonable during the growing season. Vapor pressure deficit (*VPD*) was estimated from T_a and *RH*. The growing degree days (*GDD*) were aggregated degree days when daily T_a was above 5℃ (Ueyama et al., 2013). The relative *SWC* (*SWC*r) was calculated by the following equation:

$$SWCr = \frac{SWC_{max} - SWC}{SWC_{max} - SWC_{min}} \quad (1)$$

where SWC_{max} and SWC_{min} were the maximum and minimum of measured *SWC* during the growing season in each year, respectively.

Satellite-derived vegetation indices (normalized difference vegetation index: *NDVI*; leaf area index: *LAI*; and enhanced vegetation index: *EVI*) products were acquired around the flux tower region at 1 × 1 km resolution from the Oak Ridge National Laboratory Distributed Active Archive Center (ORNL DAAC, http://daac.ornl.gov/MODIS/modis.html). 16-day *NDVI* and 16-day *EVI* were temporally interpolated to match the 8-day temporal resolution of *LAI*. We found that *EVI* was a

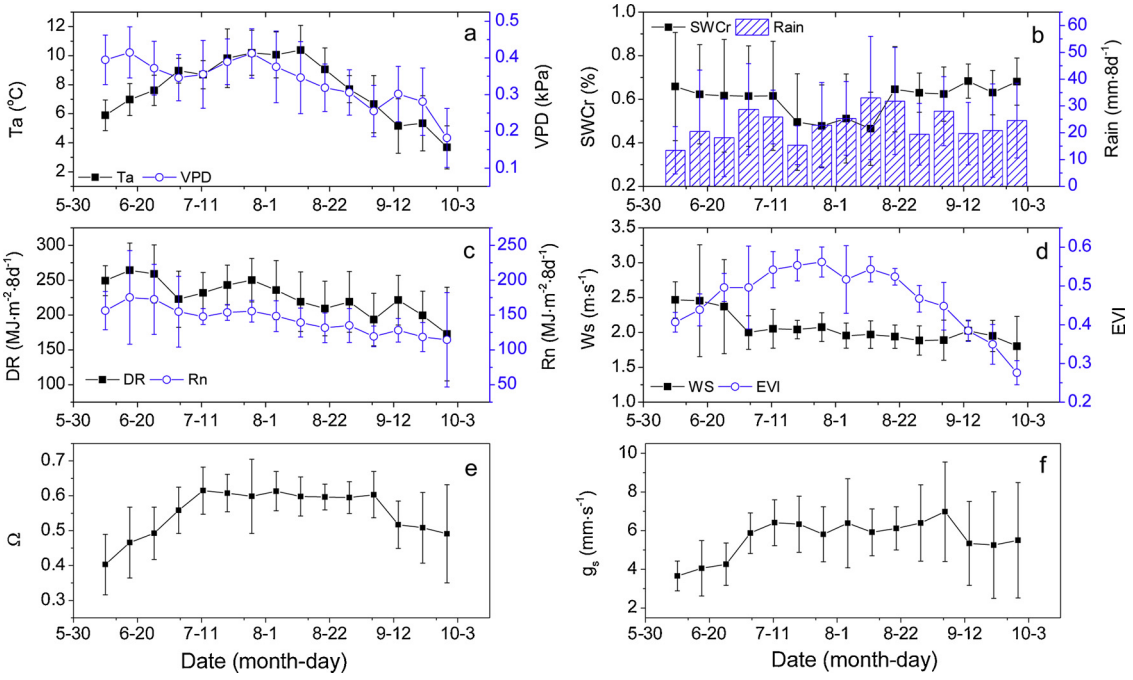

Fig. 1. The seasonal variations of 8-day air temperature (T_a) and vapor pressure deficit (*VPD*, a), relative volumetric soil water content (*SWCr*) and rainfall (*Rain*, b), incoming shortwave radiation (*DR*) and net radiation (*Rn*, c), 2.2 m wind velocity (*Ws*) and enhanced vegetation index (*EVI*, d), decoupling coefficient (Ω, e) and canopy conductance (g_s, f) in the alpine shrubland. The error bars are the standard deviation, the same below.

better index for identifying the effect of vegetation growth on seasonal variations of *ET* and *NEE*, with a little bigger R^2 than that of *NDVI* or *LAI* (Fig. S2).

2.3. Data processing

Firstly, spike screening and night-time filtering were applied to improve data quality. Spikes were defined as those outside of 4.5 standard deviations of a 10-day moving window. The night-time flux data were rejected when the corresponding friction velocity (u_*) was lower than the threshold (0.15 $m{\cdot}s^{-1}$). After spike screening and night-time filtering, the remaining valid flux data comprised 63% of the total observations. Within 10-day moving windows, *ET* gaps were filled by the linear regression of *ET* with *Rn* (Gu et al., 2008), and *NEE* gaps were filled by empirical non-linear regression of valid data with environmental variables (Li et al., 2016). To match the temporal resolution of vegetation indices, half-hour *ET*, *NEE* and the climatic variables were aggregated into 8-day balance. The aerodynamic conductance (g_a), midday bulk canopy surface conductance (g_s, from 9:00 to 16:00), and decoupling coefficient (Ω) were calculated with the methods described in the similar alpine study (Gu et al., 2008) and also screened out a small number of unrealistically high values mainly caused by rain, snow or dew events (McFadden et al., 2003).

2.4. Statistical analysis

The Shapiro-Wilk test for the 8-day dependent variables ($N = 150$) was conducted and found that *ET* ($P = 0.14$) and *NEE* ($P = 0.27$) were normally distributed without further transformation. Firstly, we fitted the 8-day *ET* and *NEE* against the Julian day with a piecewise linear function. And the lower and upper values of the 95% confidence interval were taken as the minimal and maximal capacities of *ET* and *NEE* for the growing season. Secondly, the growing season stage was considered as a dummy variable and the early growing season and the late growing season was defined as 0 and 1, respectively. Then we adopted the independent-sample *t*-test to detect the difference between environmental controls, *ET* and *NEE* during the two growth stages. Further, we performed the general linear model (GLM) with the following equation to determine whether there was a difference between two slopes from the fitted piecewise linear function during the two growth stages.

$$y = a + b \times day + c \times stage + d \times (stage \times day) + \varepsilon \quad (2)$$

where, *a* and *b* are the differential intercept and differential effect on *ET* or *ET* of the Julian day (*day*) between the two stages (*stage*), respectively. ε is a mean-zero random error item. If *c* and *d* are significantly different from 0, then the two linear slopes were significantly different (James et al., 2013).

Finally, we established structural equation models (SEMs), which can accommodate non-linear relations and non-independence effects among environmental controls, to clarify the strengths of environmental controls on *ET* and *NEE* at an 8-day temporal scale, by reporting standardized path coefficients of direct and indirect effects (Grace et al., 2012). Independent variables comprised T_a, T_{max}, T_{min}, *GDD*, *VPD*, *Ws*, *DR*, *Rn*, *Rain*, *SWCr*, and *EVI*. The SEMs were revised by theory-driven and modification indices, with thresholds usually set to 4.0. A full model including possible pathways was considered and the insignificant pathways were sequentially eliminated until the final model was achieved. The common rule of thumb that the simplest model providing an adequate fit is the best was also adopted to simplify the final model. The comparative fit index (CFI), Tucker-Lewis index (TLI), and root mean square error of approximation (RMSEA) were employed in model evaluation. The unbiased maximum likelihood method and Chi-square (χ^2) test were adopted in parameter estimation and model identification, respectively. The GLM and SEMs were performed by the glm function and Lavaan (Rosseel, 2012) packages in R 3.33 (R Development Core Team, 2006), respectively.

3. Results

3.1. Seasonal variations of environmental variables

During the growing season, the average daily T_a was 7.7 ± 2.1 °C (Mean ± 1 S.D., the same below), peaking at 10.4 ± 1.7 °C during

mid-August (Fig. 1a). Although there was little difference in T_a (P = 0.32) during the two growth stages, the 8-day *GDD* in the early growing season averaged 62.3 °C·d and was marginally significantly (P = 0.07) greater than 54.5 °C·d in the late growing season. *VPD* declined linearly (R^2 = 0.67, P < 0.001) throughout the growing season. Radiation energy also decreased linearly (R^2 > 0.67, P < 0.001), with a slightly stronger decline rate (–0.51 MJ·m^{-2}·8d^{-1}) in solar radiation than in net radiation (–0.46 MJ m^{-2}·8d^{-1}). *SWC*r exhibited a "U" pattern with its minimum from late July to mid-August (Fig. 1c), and differed insignificantly (P = 0.77) between the two stages. *EVI* showed a unimodal seasonal variation, peaking at the late July. Moreover, there was a significant (P = 0.02) difference in *EVI* between the early growing season (0.49 ± 0.08) and the late growing season (0.46 ± 0.10). The decoupling coefficient (Ω) averaged 0.55 ± 0.07, peaking at about 0.60 from mid-July to mid-August. There was not a clear seasonal pattern in surface conductance, which had a mean value of 5.62 mm·s^{-1} (Fig. 1f).

3.2. Growing season ET and NEE

The peak values of *ET* and *NEE* were 22.37 kg H_2O·m^{-2}·8d^{-1} and –21.30 g C·m^{-2}·8d^{-1}, respectively, and generally occurred at the late July with about 6-d advance in *NEE* (Fig. 2). The averaged 8-day *ET* (20.47 ± 4.54 kg H_2O·m^{-2}·8d^{-1}) and *NEE* (–12.30 ± 6.60 g C·m^{-2}·8d^{-1}) in the early growing season were significantly (P < 0.04) greater than those (16.85 ± 4.99 kg H_2O·m^{-2}·8d^{-1} and –9.53 ± 8.69 g C·m^{-2}·8d^{-1}) of the late growing season, respectively. Moreover, the slopes of *ET* and *NEE* with the Julian day were also significantly different between the two stages (Table 1), with a much more decline rate of *ET* in the late growing season and that of *NEE* in the early growing season, respectively (Fig. 2). The significant difference in *Rn* (Fig. 1)

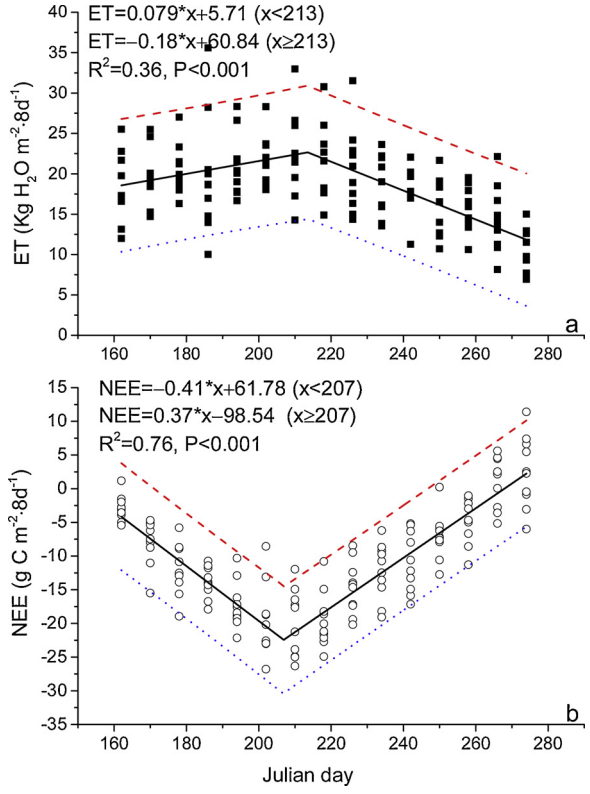

Fig. 2. The seasonal variations of accumulative 8-day evapotranspiration (*ET*, a) and 8-day net ecosystem CO_2 exchange (*NEE*, b) in the alpine shrubland. The solid regression line is for the piecewise linear function. Dashed and dotted lines show 95% confidence intervals indicated likely maximum and minimum carbon and water exchange rates.

Table 1
The general linear model of seasonal 8-day evapotranspiration (*ET*) and net ecosystem exchange (*NEE*) with growth stages, Julian day and main environmental controls during the growing season in the alpine shrubland.

Dependant	Factors	df	Mean squares	*P* value	R^2
ET	Julian day	1	96.53	P = 0.01	0.39
	Growth stages	1	723.83	P < 0.001	
	Julian × Stages	1	711.32	P < 0.001	
	Error	146	15.37		
	Rn	1	995.44	P < 0.001	0.46
	Growth stages	1	90.52	P = 0.01	
	Rn × Stages	1	107.03	P = 0.006	
	Error	146	13.52		
	VPD	1	1430.37	P < 0.001	0.58
	Growth stages	1	1.63	P = 0.70	
	VPD × Stages	1	1.83	P = 0.68	
	Error	146	10.64		
NEE	Julian day	1	13.35	P = 0.35	0.77
	Growth stages	1	5698.38	P < 0.001	
	Julian × Stages	1	5206.29	P < 0.001	
	Error	146	15.35		
	EVI	1	3,605.87	P < 0.001	0.60
	Growth stages	1	84.08	P = 0.077	
	EVI × Stages	1	78.86	P = 0.087	
	Error	146	26.56		
	GDD	1	2320.23	P < 0.001	0.44
	Growth stages	1	0.29	P = 0.93	
	GDD × Stages	1	2.66	P = 0.79	
	Error	146	36.36		

and in its slope versus *ET* (Table 1 and Fig. 3a, b) between the two growth stages, suggested that *Rn* more than *VPD* probably accounted for the asymmetric behavior in *ET*. Similarly, *EVI* may be much more important than *GDD* in explaining this asymmetric manner in *NEE* (Table 1 and Fig. 3c, d). Extrapolating the data for the whole growing season showed that the accumulative *ET* water loss averaged 278.1 ± 16.9 mm, with a maximum of 408.0 mm and a minimum of 161.4 mm at 95% confidence. The water budget (the difference between the precipitation amounts and cumulative *ET*) thus averaged 62.3 ± 50.3 mm. The carbon sequestration capacity (–*NEE*) averaged 159.6 ± 28.3 g C·m^{-2} and its maximum and minimum was 278.4 g C·m^{-2} and 41.0 g C·m^{-2}, respectively. The alpine shrubland ecosystem thus acted as a water source and a carbon sink during the growing season. The ecosystem water use efficiency (*WUE*, –*NEE*/*ET*) averaged 0.60 ± 0.32 g C·kg H_2O^{-1} and followed a bell-shape seasonal pattern, peaking in the early August (0.92 ± 0.19 g C·kg H_2O^{-1}). GLM of *WUE* with *ET* and *NEE* indicated that *NEE,* more than *ET,* dominated *WUE* seasonal variability, with a larger standard regression coefficient (Table 2). *WUE* changed insignificantly (P = 0.94) between the two growth stages.

3.3. Determinants on seasonal variations of ET and NEE

The structural equation models (SEMs) for 8-day *ET* (Chi-square (χ^2) = 8.97, P = 0.26; note that a significant (P < 0.05) χ^2 calls for rejection of the proposed model) and 8-day *NEE* (χ^2 = 13.46, P = 0.14) were all identified. The SEMs explained 73% and 69% seasonal variations in *ET* and *NEE* (Fig. 4), respectively, not more than the explanatory power of GLM (Table 2). *VPD* and *Rn* exerted almost the equivalent influence on seasonal variations of *ET*, but the total effect of *VPD* was only 0.34 (= 0.61 + 0.59 × –0.46). *EVI* only showed a weakly positive impact on *ET* seasonal variability (Fig. 4a). The largest direct effect on *NEE* was from *EVI,* followed by *GDD* and *DR*, with standard coefficients of –0.51, –0.46 and –0.45, respectively (Fig. 4b). However, the total effect of *GDD* reached –0.79 (= –0.46 + 0.64 × –0.51), indicating that *GDD* played a comprehensive dominant role in *NEE* seasonal variability. Therefore, variations of *ET* and *NEE* were much directly regulated by *Rn* and *EVI* during the growing season,

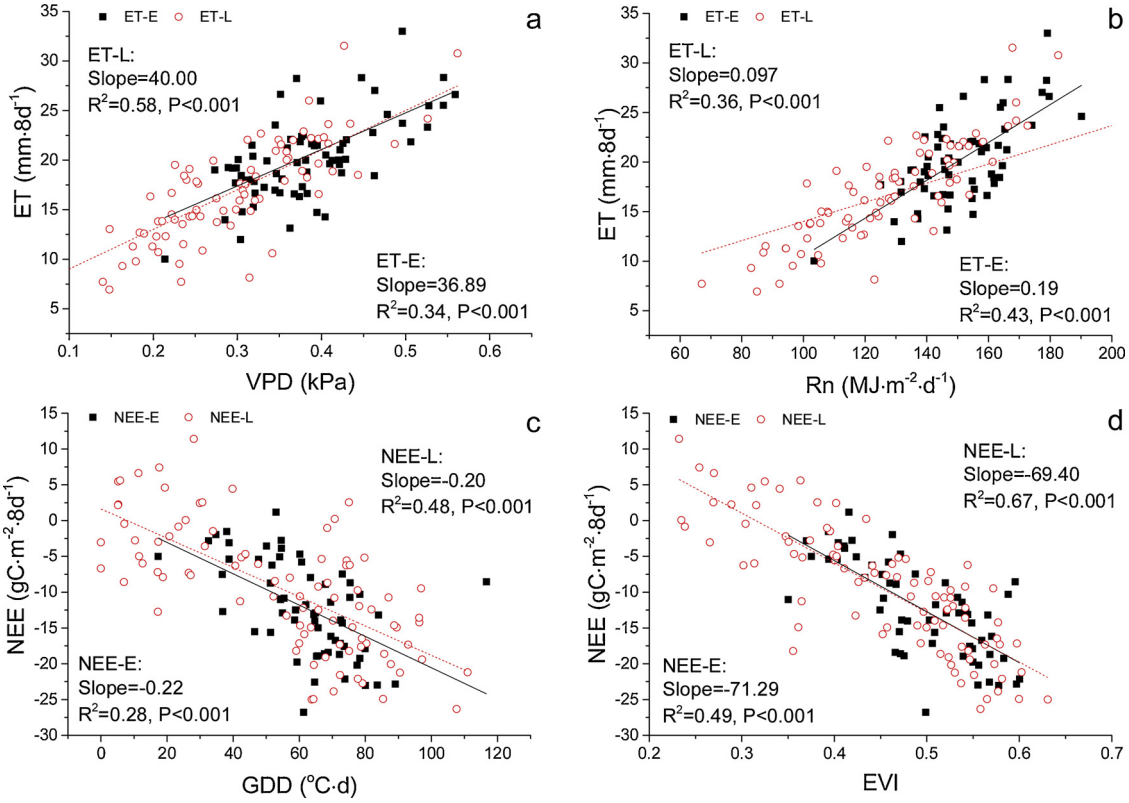

Fig. 3. The relationship between 8-day evapotranspiration (*ET*) with vapor pressure deficit (*VPD*, a) and net radiation (*Rn*, b) and the relationship between 8-day net ecosystem exchange (*NEE*) with aggregated growing daily degrees (*GDD*, c) and enhanced vegetation index (*EVI*, d) during the early growing season (suffixed "-E") and the late growing season (suffixed "-L") in the alpine shrubland. The solid and dotted regression lines indicate the early growing season and late growing season, respectively.

Table 2
The general linear model of seasonal 8-day evapotranspiration (*ET*) and net ecosystem exchange (*NEE*) with main environmental controls during the growing season in the alpine shrubland.

Dependant	Factors	Standard regression coefficients	*P* value	R^2	
ET	*Rn*	0.31	$P = 0.07$	0.70	The whole
	VPD	0.036	$P = 0.35$		growing season
	Rn × *VPD*	0.028	$P < 0.001$		(N = 150)
	Rn#	0.38	$P = 0.001$	0.51	The early
	VPD#	0.42	$P < 0.001$		growing season
	Rn × *VPD*#	—	—		(N = 70)
	Rn	0.16	$P = 0.26$	0.76	The late
	VPD	–0.30	$P = 0.08$		growing season
	Rn × *VPD*	1.06	$P < 0.001$		(N = 80)
NEE	*EVI*	–0.73	$P < 0.001$	0.64	The whole
	GDD	–0.30	$P = 0.24$		growing season
	EVI × *GDD*	0.18	$P = 0.58$		(N = 150)
	EVI	–1.33	$P = 0.002$	0.42	The early
	GDD	–1.84	$P = 0.007$		growing season
	EVI × *GDD*	2.26	$P = 0.019$		(N = 60)
	EVI	–0.67	$P < 0.001$	0.69	The late
	GDD	–0.20	$P = 0.53$		growing season
	EVI × *GDD*	–0.002	$P = 0.99$		(N = 90)
*WUE***	*NEE*	–1.86	$P < 0.001$	0.98	The whole
	ET	–0.12	$P < 0.001$		growing season
	NEE × *ET*	0.96	$P < 0.001$		(N = 132)

Note: "**" represents that the data size of WUE_n is 132 because the positive NEE value is omitted, "#" is the regression model without interaction item because none of the effects in the full model is significant ($0.38 < P < 0.82$).

respectively. The remarkably different effects of *EVI* on *ET* and *NEE* probably indicated that water loss and carbon fixation was weakly coupled in the humid alpine shrubland. Annually, none of the environmental controls could significantly ($P > 0.12$) account for the year-to-year variations of growing season *ET* and *NEE* (Tab.S1).

4. Discussions

4.1. The asymmetric behavior of ET and NEE during the two growth stages

We found that the magnitude and sensitivity in *ET* and *NEE* were significantly different between the early growing season and the late growing season (Table 1 and Fig. 2), which were also documented over other alpine grasslands (Körner, 2003; Ma et al., 2015; Li et al., 2017). The asymmetric behavior of *ET* during the two growth stages could reflect the combination of radiation energy availability and atmospheric humidity deficit, but not the influence of surface moisture supply (Table 2 and Fig. 4a). The infrequent soil moisture competition between deep-rooted shrubs and shallow-rooted grass, and high soil water-holding capacity of the abundant topsoil organic matter would together reflect that the shrubland would not expect to experience heave water stress with respect to *ET* under synchronized rainfall and temperature climate (Iwata et al., 2012; Shao et al., 2015). *ET* seasonal variability thus was determined by the atmospheric evaporative demand (Chapin et al., 2011), the combination of *Rn* and *VPD* (Fig. 4a). The further GLM of *ET* with *VPD* (*Rn*) and the growth stages revealed that *Rn* ($P = 0.006$), rather than *VPD* ($P = 0.68$), was more closely related to this seasonal asymmetric pattern in *ET* (Fig. 3a, b, and Table 1). The underlying mechanism might be the increased *ET* in the early growing season could result in a gradual increase in cloud coverage, which could depress the net radiation and humidity deficit during the subsequent late growing season (Chapin et al., 2005; Ma

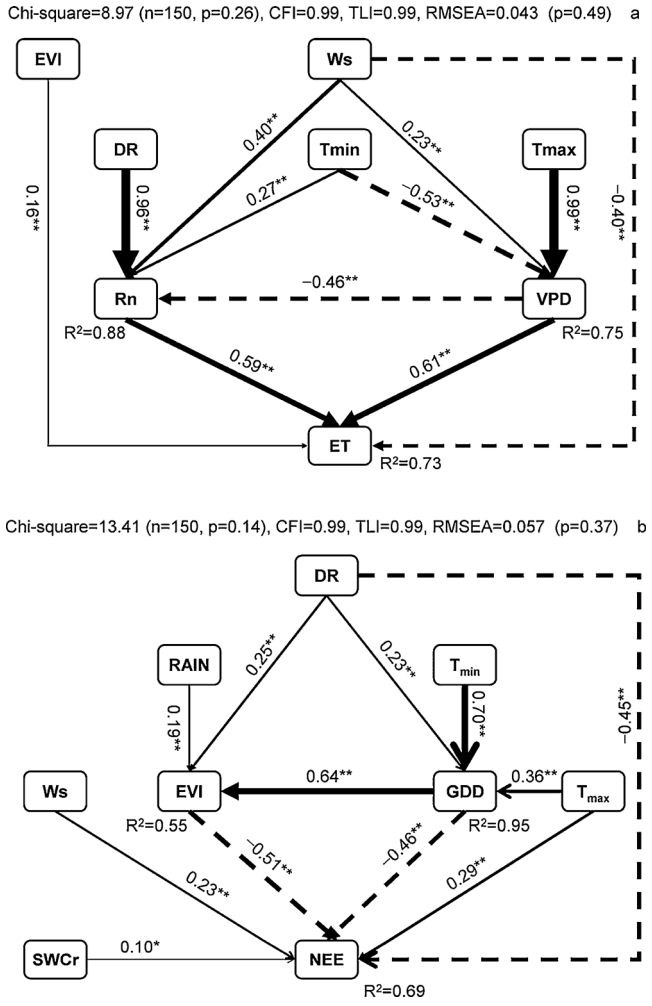

Fig. 4. Structural equation models for seasonal 8-day evapotranspiration *ET* (a) and *NEE* (b) during growing season in the alpine shrubland (solid and dotted lines represent positive and negative paths; values near the arrows are the standard path coefficient, and the line weight is ten times the standard effect sizes. **and * represent $P < 0.01$ and $P < 0.05$, respectively. Abbreviations: T_{max} and T_{min}: daily maximum and minimum air temperature; *SWC*r: relative 5 cm soil water content; *VPD*: vapor pressure deficit; *EVI*: enhanced vegetation index; *DR*: solar radiation; *Rn*: net radiation; *Ws*: wind velocity; CFI: comparative fit index; TLI: Tucker-Lewis index; RMSEA: root mean square error of approximation.

et al., 2015). This explanation was also supported by the lower slope of *ET* with *Rn* during the late growing season (Fig. 3; Iwata et al., 2012). The significant declining *Rn* and *VPD* throughout the growing season were seemed to corroborate the above speculation (Fig. 1).

The asymmetric characteristic in *NEE* could be largely attributed to changes in thermal conditions (*GDD*) and vegetation growth (*EVI*), not soil water content either (Fig. 4 and Table 2). However, GLM of *NEE* with *GDD* and the growth stages showed that there was little significant difference ($P = 0.93$) in the slopes of *NEE* against *GDD* during the two stages (Fig. 3 and Table 1), indicating that the thermal conditions should not be the main cause of this asymmetric manner. Therefore, the vegetation growth status may be one good reference in explaining the asymmetric *NEE* variability (Li et al., 2017). The result of the only significant effect of *EVI* ($P < 0.001$) from GLM of *NEE* with *EVI* and *GDD* partly confirmed this supposition (Table 2). While further analysis of GLM of *NEE* with growth stages and *EVI* showed that the effect of growth stages ($P = 0.077$) and their interaction ($P = 0.087$) was also marginally significant (Table 2), suggesting that the *EVI* alone could not enough account for this asymmetric manner.

The growth stages-related nitrogen allocation strategies to accommodate the short growing length (Körner, 2003; Li et al., 2017) might be complementary and alpine plants generally distribute much nitrogen in new photosynthetic tissues during the early growing season and translocate N from green leaves to non-photosynthetic tissues (roots and fruits) in the late growing season (Körner, 2003). The majority of leaf nitrogen is associated with chlorophyll and other photosynthetic molecules, and plays an important function in maintaining plant photosynthesis (Chapin et al., 2011) and in sustaining the plasticity in photosynthetic capacity, which is much stronger than that of temperate plant species (Rogers et al., 2017). This explanation agreed well with that warmer conditions in the early growing season, more than in the late growing season (Table 2), could stimulate photosynthetic activity in alpine plants (Körner, 2003; Li et al., 2016). Meanwhile, we also observed that the grass leaf N concentrations of 32.99 $g \cdot kg^{-1}$ and 30.30 $g \cdot kg^{-1}$ in the early growing season of May and July, which were greater than their values of 16.85 $g \cdot kg^{-1}$ and 17.07 $g \cdot kg^{-1}$ in the late growing season of September and November (personal observation data). Consequently, we speculated that vegetation growth and associated leaf nitrogen concentrations (Li et al., 2017) could be mostly attributed to the asymmetric seasonal variations of *NEE*. The results indicated that it would be a little unreasonable that generally assuming a certain value of leaf nitrogen concentrations in carbon model simulations in alpine grasslands.

While the significant difference in the magnitude of *ET* and *NEE* was small between the two growth stages in the alpine shrubland (Table 1 and Fig. 2), the large spatial extent of this ecosystem type (Zheng et al., 2000) allowed their asymmetric behaviors to be important characteristics of the water and carbon budgets across the QTP. Moreover, our results revealed the response of the dynamics of water vapor and CO_2 to future warming scenarios could be growth stage-dependent. Specifically, given higher leaf N concentrations, warming in the early growing season would facilitate the carbon sequestration capacity whereas the corresponding impact during the late growing season might be attenuated by stimulated earlier leaf senescence and lower canopy N concentrations (Kato et al., 2006; Li et al., 2017). This was in good line with observations that the sensitivity of gross primary production (*GPP*) to spring temperature is greater than that to autumn temperature (Piao et al., 2008; Ueyama et al., 2014). Additionally, the slope (730.4 g $C \cdot m^{-2} \cdot month^{-1}$) of monthly *GPP* with *EVI* in the early growing season was also much greater than that (447.2 g $C \cdot m^{-2} \cdot month^{-1}$) of the late growing season, implying that different vegetation photosynthetic efficiency was likely induced by the changing canopy nitrogen concentrations (Li et al., 2016). The asymmetric behavior during the early growing season and the late growing season might be important for reducing uncertainties when modelling carbon budgets (Le Quéré et al., 2009), because the growth stage-dependent grazing management and future warming scenarios are likely to be the important controls on the carbon balance of temperature-limited grasslands (Ueyama et al., 2013).

4.2. Differential controls of EVI on ET and NEE

Although there was a significant positive relationship between *ET* and vegetation indices (Fig. S2), this likely stemmed from the seasonal coincidence between radiation energy availability and vegetation growth in cold regions (Vourlitis and Oechel, 1999; Blok et al., 2011). Moreover, the weak correlation ($R^2 = 0.02$, $P = 0.04$, $N = 150$) between g_s and *ET* seemed to imply that biological constraint of stomatal behavior on *ET* was small (Vourlitis and Oechel, 1999; Ma et al., 2015). The phenotypic potential for the weak effect of *EVI* on *ET* (Fig. 4a) may arise from a much earlier canopy closure caused by the prostrate vegetation growth form of most alpine plants, with little effect on the underlying surface roughness (Körner, 2003) and surface albedo or on the resultant surface energy partitioning (Gu et al., 2008; Richardson et al., 2013). Consequently, *ET* was much regulated by *Rn*, more than

VPD and *EVI*, reflecting an energy-limited condition for *ET* during the growing season in humid alpine grasslands (Knowles et al., 2012; Ma et al., 2015; Zhang et al., 2018).

Alpine vegetation growth is closely related to thermal conditions, which result in the strong correlation between *GDD* and *EVI* (Fig. 4b) at higher productivity sites (Kato et al., 2006; Ueyama et al., 2013). Therefore, *EVI*, more than *GDD*, could be a key direct driver in the seasonal variability of gross primary production (Kato et al., 2006; Ueyama et al., 2013) and the resultant *NEE* (McGuire et al., 2002; Li et al., 2016) in alpine grasslands. This can be explained by the combination of vegetation photosynthetic capacity increasing with *EVI*, as well as leaf maintenance respiration and soil respiration also constraining with substrate mainly from photosynthetic products in colder sites (McFadden et al., 2003; Li et al., 2016). Moreover, warming treatments could stimulate a more increasing photosynthesis while respiratory acclimation under moist conditions (Körner, 2003; Chen et al., 2016), which also contributed to the direct influence of *EVI* on *NEE*. The more important direct role of *EVI* on *NEE* agreed well with the observation that biotic controls were more important than abiotic drivers in determining *NEE* variability under humid conditions (Shao et al., 2015). However, the insignificant annual correlation (Tab S1) of *ET* with *Rn* ($P = 0.18$) and *NEE* with *EVI* ($P = 0.50$) indicated a scale-dependent variability in water vapor and CO_2 exchanges in the alpine shrubland.

4.3. Poor coupling of ET and NEE

The weak coupling between *ET* and *NEE* was also found in the cold environment of Alaska (Vourlitis and Oechel, 1999; McFadden et al., 2003), perhaps because the common feature in alpine shrubland is the high fractions of *ET* derived from moss surfaces, with *NEE* reflecting the activity of vascular plants (Vourlitis and Oechel, 1999; McGuire et al., 2002; Blok et al., 2011). The results of the Shuttleworth–Wallace two-source model partly confirmed that surface evaporation was about 40% *ET* during the growing season at the same site (Hu et al., 2009). Moreover, the monthly surface conductance (g_s) ranged from 2.33 $mm{\cdot}s^{-1}$ to 7.87 $mm{\cdot}s^{-1}$ and was much lower than the model prediction (ca. 15 $mm{\cdot}s^{-1}$ based on the maximum leaf conductance 5 $mm{\cdot}s^{-1}$, Kelliher et al., 1995). This discrepancy in g_s was probably explained by the exponential decrease in water vapor exchange and soil conductance when tissue water decreased in mosses (McFadden et al., 2003; Blok et al., 2011). To some extent, monthly g_s was correlated with monthly rainfall ($R^2 = 0.33$, $P < 0.001$, $N = 40$), not *SWC* ($R^2 = 0.001$, $P = 0.84$) or *EVI* ($R^2 = 0.05$, $P = 0.10$), in part reflecting that the abundance and activity of cryptogams are generally related positively with rainfall events (Vourlitis and Oechel, 1999; Blok et al., 2011). Consistent with this explanation, we found that *NEE* rather than *ET* played a much more important function in *WUE* seasonal variability (Table 2). Meanwhile, the peak *WUE* was half and two-thirds of the unconstrained intrinsic leaf-level *WUE* of *Potentilla fruticosa* shrub (ca. 3.0 μmol $CO_2{\cdot}mmol\ H_2O^{-1}$) and dominant grasses (ca. 1.8 μmol $CO_2{\cdot}mmol\ H_2O^{-1}$), respectively, suggesting that the water loss might about half originate from evaporation. In addition, the canopy interception ratio of rainfall could be up to 20% in humid alpine grasslands with higher plant coverage and be readily re-evaporated under strong solar radiation on the Plateau (Wang et al., 2012). In summary, about half *ET* might be derived from soil, moss and canopy interception evaporation, together with distinct environmental controls of *ET* and *NEE*, result in the poor coupling between water loss and carbon fixation in the alpine shrubland.

5. Conclusions

Our results revealed in the magnitude and sensitivities of *ET* and *NEE* between the early growing season and the late growing season changed significantly. Such asymmetric behavior probably resulted from the differential net radiation and vegetation growth during the two stages, respectively. Moreover, the direct effect of *EVI* on *ET* was much less than that on *NEE,* implying decoupling water vapor loss and carbon fixation in the humid alpine shrubland. Our findings have two important implications for predicting future water resource and carbon function. First, there were significant differential responses of water vapor and CO_2 exchanges during the two growth stages. The reasonable temporal resolution in seasonal variations of vegetation growth and canopy N concentration and net radiation availability should be needed in future projections in humid alpine shrublands. The relationship between ecosystem carbon budgets and vegetation growth may be growth stage-dependent and constrained by the plant's N distribution strategy in humid alpine shrubland, making the responses of carbon sequestration to vegetation coverage changes induced by grazing duration and future climate change more complex. Second, the vegetation status played different roles in water vapor and CO_2 exchanges in humid alpine shrubland, which is in contrast to the prevailing view of a tight coupling between water and carbon processes. The differential role of moss abundance in water and carbon dynamics would be taken into enough considerations in humid alpine shrublands.

Author contributions

H Li, J Zhu, and F Zhang performed the research, analyzed data, and wrote the paper; H He, Y Yang, G Cao, and H Zhou analyzed data and wrote the paper, and Y Li conceived the study.

Conflict of interest

The authors declare no conflict of interest.

Acknowledgments

This work was financially supported by the National Key R&D Program (2017YFA0604801), the National Natural Science Foundation of China (41730752, 41877547), Qinghai R&D Infrastructure and Facility Development Program (2018-ZJ-T09), and Qinghai Innovation Platform Construction Project (2017-ZJ-Y20).

Appendix A. Supplementary data

Supplementary material related to this article can be found, in the online version, at doi:https://doi.org/10.1016/j.agrformet.2019.01.013.

References

Blok, D., Heijmans, M.M.P.D., Schaepman-Strub, G., van Ruijven, J., Parmentier, F.J.W., Maximov, T.C., Berendse, F., 2011. The cooling capacity of mosses: controls on water and energy fluxes in a Siberian Tundra site. Ecosystems 14, 1055–1065. https://doi.org/10.1007/s10021-011-9463-5.

Chapin, F.S., Sturm, M., Serreze, M.C., McFadden, J.P., Key, J.R., Lloyd, A.H., McGuire, A.D., Rupp, T.S., Lynch, A.H., Schimel, J.P., Beringer, J., Chapman, W.L., Epstein, H.E., Euskirchen, E.S., Hinzman, L.D., Jia, G., Ping, C.L., Tape, K.D., Thompson, C.D.C., Walker, D.A., Welker, J.M., 2005. Role of land-surface changes in arctic summer warming. Science 310, 657. https://doi.org/10.1126/science.1117368.

Chapin, F.S., Matson, P.A., Mooney, H.A., 2011. Principles of Terrestrial Ecosystem Ecology. Springer-Verlag, New York, USA, pp. 142–145.

Chen, J., Luo, Y., Xia, J., Shi, Z., Jiang, L., Niu, S., Zhou, X., Cao, J., 2016. Differential responses of ecosystem respiration components to experimental warming in a meadow grassland on the Tibetan Plateau. Agr. Forest Meteorol. 220, 21–29. https://doi.org/10.1016/j.agrformet.2016.01.010.

Grace, J.B., Schoolmaster, D.R., Guntenspergen, G.R., Little, A.M., Mitchell, B.R., Miller, K.M., Schweiger, E.W., 2012. Guidelines for a graph-theoretic implementation of structural equation modeling. Ecosphere 3, 1–44. https://doi.org/10.1890/ES12-00048.1.

Gu, S., Tang, Y., Cui, X., Du, M., Liang, Z., Li, Y., Xu, S., Zhou, H., Kato, T., Qi, P., 2008. Characterizing evapotranspiration over a meadow ecosystem on the Qinghai-Tibetan Plateau. J. Geophys. Res.-Atmos. 113. https://doi.org/10.1029/2007JD009173.

Hu, Z., Yu, G., Zhou, Y., Sun, X., Li, Y., Shi, P., Wang, Y., Song, X., Zheng, Z., Zhang, L., Li, S., 2009. Partitioning of evapotranspiration and its controls in four grassland

ecosystems: application of a two-source model. Agr. Forest Meteorol. 149, 1410–1420. https://doi.org/10.1016/j.agrformet.2009.03.014.
Iwata, H., Harazono, Y., Ueyama, M., 2012. The role of permafrost in water exchange of a black spruce forest in Interior Alaska. Agr. Forest Meteorol. 161, 107–115. https://doi.org/10.1016/j.agrformet.2012.03.017.
James, G., Witten, D., Hastie, T., Tibshirani, R., 2013. An Introduction to Statistical Learning- With Applications in R. Springer-Verlag, New York, USA.
Kato, T., Tang, Y.H., Gu, S., Hirota, M., Du, M.Y., Li, Y.N., Zhao, X.Q., 2006. Temperature and biomass influences on interannual changes in CO_2 exchange in an alpine meadow on the Qinghai-Tibetan Plateau. Glob. Change Biol. Bioenergy 12, 1285–1298. https://doi.org/10.1111/j.1365-2486.2006.01153.x.
Kelliher, F.M., Leuning, R., Raupach, M.R., Schulze, E.D., 1995. Maximum conductances for evaporation from global vegetation types. Agr. Forest Meteorol. 73, 1–16. https://doi.org/10.1016/0168-1923(94)02178-M.
Knowles, J.F., Blanken, P.D., Williams, M.W., Chowanski, K.M., 2012. Energy and surface moisture seasonally limit evaporation and sublimation from snow-free alpine tundra. Agr. Forest Meteorol. 157, 106–115. https://doi.org/10.1016/j.agrformet.2012.01.017.
Körner, C., 2003. Alpine Plant Life: Functional Plant Ecology of High Mountain Ecosystems. Springer-Verlag, Berlin Heidelberg.
Le Quéré, C., Raupach, M.R., Canadell, J.G., Marland, G., Bopp, L., Ciais, P., Conway, T.J., Doney, S.C., Feely, R.A., Foster, P., Friedlingstein, P., Gurney, K., Houghton, R.A., House, J.I., Huntingford, C., Levy, P.E., Lomas, M.R., Majkut, J., Metzl, N., Ometto, J.P., Peters, G.P., Prentice, I.C., Randerson, J.T., Running, S.W., Sarmiento, J.L., Schuster, U., Sitch, S., Takahashi, T., Viovy, N., van der Werf, G.R., Woodward, F.I., 2009. Trends in the sources and sinks of carbon dioxide. Nat. Geosci. 2, 831–836. https://doi.org/10.1038/ngeo689.
Li, H., Zhang, F., Li, Y., Cao, G., Zhao, L., Zhao, X., 2014. Seasonal and interannual variations of ecosystem photosynthetic features in an alpine dwarf shrubland on the Qinghai-Tibetan Plateau, China. Photosynthetica 52, 321–331. https://doi.org/10.1007/s11099-014-0035-8.
Li, H., Zhang, F., Li, Y., Wang, J., Zhang, L., Zhao, L., Cao, G., Zhao, X., Du, M., 2016. Seasonal and inter-annual variations in CO_2 fluxes over 10 years in an alpine shrubland on the Qinghai-Tibetan Plateau, China. Agr. Forest Meteorol. 228–229, 95–103. https://doi.org/10.1016/j.agrformet.2016.06.020.
Li, F., Peng, Y., Natali, S.M., Chen, K., Han, T., Yang, G., Ding, J., Zhang, D., Wang, G., Wang, J., Yu, J., Liu, F., Yang, Y., 2017. Warming effects on permafrost ecosystem carbon fluxes associated with plant nutrients. Ecology 98, 2851–2859. https://doi.org/10.1002/ecy.1975.
McFadden, J.P., Eugster, W., Chapin, F.S., 2003. A regional study of the controls on water vapor and CO_2 exchange in arctic tundra. Ecology 84, 2762–2776. https://doi.org/10.1890/01-0444.
McGuire, A.D., Wirth, C., Apps, M., Beringer, J., Clein, J., Epstein, H., Kicklighter, D.W., Bhatti, J., Chapin, F.S., de Groot, B., Efremov, D., Eugster, W., Fukuda, M., Gower, T., Hinzman, L., Huntley, B., Jia, G.J., Kasischke, E., Melillo, J., Romanovsky, V., Shvidenko, A., Vaganov, E., Walker, D., 2002. Environmental variation, vegetation distribution, carbon dynamics and water/energy exchange at high latitudes. J. Veg. Sci. 13, 301–314. https://doi.org/10.1111/j.1654-1103.2002.tb02055.x.
Piao, S., Ciais, P., Friedlingstein, P., Peylin, P., Reichstein, M., Luyssaert, S., Margolis, H., Fang, J., Barr, A., Chen, A., Grelle, A., Hollinger, D.Y., Laurila, T., Lindroth, A., Richardson, A.D., Vesala, T., 2008. Net carbon dioxide losses of northern ecosystems in response to autumn warming. Nature 451, 49–52. https://doi.org/10.1038/nature06444.
R Development Core Team, 2006. R: a Language and Environment for Statistical Computing. R foundation for statistical computing, Vienna.
Richardson, A.D., Keenan, T.F., Migliavacca, M., Ryu, Y., Sonnentag, O., Toomey, M., 2013. Climate change, phenology, and phenological control of vegetation feedbacks to the climate system. Agr. Forest Meteorol. 169, 156–173. https://doi.org/10.1016/j.agrformet.2012.09.012.
Rogers, A., Serbin, S.P., Ely, K.S., Sloan, V.L., Wullschleger, S.D., 2017. Terrestrial biosphere models underestimate photosynthetic capacity and CO_2 assimilation in the Arctic. New Phytol. 216, 1090–1103. https://doi.org/10.1111/nph.14740.
Rosseel, Y., 2012. Lavaan: an r package for structural equation modeling. J. Stat. Softw. 48, 1–36.
Shao, J., Zhou, X., Luo, Y., Li, B., Aurela, M., Billesbach, D., Blanken, P.D., Bracho, R., Chen, J., Fischer, M., Fu, Y., Gu, L., Han, S., He, Y., Kolb, T., Li, Y., Nagy, Z., Niu, S., Oechel, W.C., Pinter, K., Shi, P., Suyker, A., Torn, M., Varlagin, A., Wang, H., Yan, J., Yu, G., Zhang, J., 2015. Biotic and climatic controls on interannual variability in carbon fluxes across terrestrial ecosystems. Agr. Forest Meteorol. 205, 11–22. https://doi.org/10.1016/j.agrformet.2015.02.007.
Shen, M., Piao, S., Jeong, S., Zhoue, L., Zeng, Z., Ciais, P., Chen, D., Huang, M., Jin, C., Li, L.Z.X., Li, Y., Myneni, R.B., Yang, K., Zhang, G., Zhang, Y., Yao, T., 2015. Evaporative cooling over the Tibetan Plateau induced by vegetation growth. Proc. Natl. Acad. Sci. U. S. A. 112, 9299–9304. https://doi.org/10.1073/pnas.1504418112.
Teuling, A.J., Seneviratne, S.I., Stockli, R., Reichstein, M., Moors, E., Ciais, P., Luyssaert, S., van den Hurk, B., Ammann, C., Bernhofer, C., Dellwik, E., Gianelle, D., Gielen, B., Grunwald, T., Klumpp, K., Montagnani, L., Moureaux, C., Sottocornola, M., Wohlfahrt, G., 2010. Contrasting response of European forest and grassland energy exchange to heatwaves. Nat. Geosci. 3, 722–727. https://doi.org/10.1038/ngeo950.
Ueyama, M., Iwata, H., Harazono, Y., Euskirchen, E.S., Oechel, W.C., Zona, D., 2013. Growing season and spatial variations of carbon fluxes of Arctic and boreal ecosystems in Alaska(USA). Ecol. Appl. 23, 1798–1816. https://doi.org/10.1890/11-0875.1.
Ueyama, M., Iwata, H., Harazono, Y., 2014. Autumn warming reduces the CO_2 sink of a black spruce forest in interior Alaska based on a nine-year eddy covariance measurement. Glob. Change Biol. Bioenergy 20, 1161–1173. https://doi.org/10.1111/gcb.12434.
Vourlitis, G.L., Oechel, W.C., 1999. Eddy covariance measurements of CO_2 and energy fluxes of an Alaskan tussock tundra ecosystem. Ecology 80, 686–701. https://doi.org/10.1890/0012-9658(1999)080. [0686:ECMOCA]2.0.CO;2.
Wang, G., Liu, G., Li, C., 2012. Effects of changes in alpine grassland vegetation cover on hillslope hydrological processes in a permafrost watershed. J. Hydrol. (Amst) 444-445, 22–33. https://doi.org/10.1016/j.jhydrol.2012.03.033.
Zhang, F., Li, H., Wang, W., Li, Y., Lin, L., Guo, X., Du, Y., Li, Q., Yang, Y., Cao, G., Li, Y., 2018. Net radiation rather than moisture supply governs the seasonal variations of evapotranspiration over an alpine meadow on the northeastern Qinghai-Tibetan Plateau. Ecohydrology 11, e1925. https://doi.org/10.1002/eco.1925.
Zheng, D., Zhang, Q.S., Wu, S.H., 2000. Mountain Geoecology and Sustainable Development of the Tibetan Plateau. Kluwer Academic, Dordercht, the Netherlands.